Comparison of current-driven and conductance-driven neocortical model neurons with Hodgkin-Huxley voltage-gated channels

P. H. E. Tiesinga,[1,*] Jorge V. José,[2] and Terrence J. Sejnowski[1,3]
[1]*Sloan Center for Theoretical Neurobiology and Computational Neurobiology Laboratory, Salk Institute, 10010 North Torrey Pines Road, La Jolla, California 92037*
[2]*Center for Interdisciplinary Research on Complex Systems and Department of Physics, Northeastern University, 360 Huntington Avenue, Boston, Massachusetts 02115*
[3]*Department of Biology, University of California–San Diego, La Jolla, California 92093*
(Received 1 June 2000)

Intrinsic noise and random synaptic inputs generate a fluctuating current across neuron membranes. We determine the statistics of the output spike train of a biophysical model neuron as a function of the mean and variance of the fluctuating current, when the current is white noise, or when it derives from Poisson trains of excitatory and inhibitory postsynaptic conductances. In the first case, the firing rate increases with increasing variance of the current, whereas in the latter case it decreases. In contrast, the firing rate is independent of variance (for constant mean) in the commonly used random walk, and perfect integrate-and-fire models for spike generation. The model neuron can be in the current-dominated state, representative of neurons in the *in vitro* slice preparation, or in the fluctuation-dominated state, representative of *in vivo* neurons. We discuss the functional relevance of these states to cortical information processing.

PACS number(s): 87.19.La, 87.17.Nn, 87.17.Aa

I. INTRODUCTION

The random-walk (RW) [1,2], and integrate-and-fire (IAF) models [3] were introduced to account for the stochastic discharge of neurons that was measured experimentally. Recently, the highly variable discharge of cortical neurons *in vivo* has led to renewed interest in these models [4–8]. *In vivo* neocortical neurons undergo a constant bombardment by excitatory and inhibitory postsynaptic potentials (EPSPs and IPSPs). Under these conditions, the IAF model neuron produces a regular spike train (low coefficient of variation, $C_V \ll 1$, see below), whereas in the cortex the neurons actually fire with a $C_V \approx 1$ [4]. A number of modifications of the standard IAF have been proposed to make it spike at a higher C_V, such as balanced excitatory and inhibitory synaptic inputs [5,8], physiological gain [9], and partial reset after an emitted spike [10]. The issue of high C_V values has, however, only partially been addressed using more realistic biophysical model neurons [8,11,12]. How do the C_V values of the neuronal discharge of a biophysical neuron depend on the statistical characteristics of its fluctuating input current? How is the neuron's *in vivo* dynamics different from that in the *in vitro* preparation?

Here we address these two issues theoretically. We systematically study a biophysical model neuron with Hodgkin-Huxley voltage-gated channels. The model neuron produces short duration action potentials with a fast after-hyperpolarization, and it can fire at high sustained firing rates, consistent with the properties of regular and fast spiking cortical neurons [13]. We apply to the model neuron two fluctuating current drives: a white-noise current with mean I and variance D, and a Poisson train of excitatory and inhibitory postsynaptic conductances, characterized by mean η and variance η_2 of the resulting synaptic currents. The main result is that the source of the fluctuating currents matters: The firing rate is differently affected by the variance, D, of a white-noise current drive compared to the variance η_2 of a conductance drive. The commonly used RW model does not account for this effect of the variance on the firing rate. Also, the model neuron can be in the fluctuation- or current-dominated state depending on the value of the variance. The potential information encoding capacity of the neuron is qualitatively different in these states.

II. METHODS

A. Model equations

The neuron is modeled as a single compartment with Hodgkin-Huxley-type voltage-gated sodium and potassium currents, with the rate functions and values for the maximum conductances as given in Ref. [14]. Briefly, the equation for the membrane potential V of a neuron is

$$C_m \frac{dV}{dt} = -I_{\mathrm{Na}} - I_{\mathrm{K}} - I_{\mathrm{L}} - I_{\mathrm{syn}} + I_{\mathrm{app}} + C_m \xi. \qquad (1)$$

Here I_{Na}, I_{K}, I_L, I_{syn}, I_{app}, and $C_m\xi$ are the sodium, potassium, leak, synaptic, externally applied, and noise currents, respectively. A detailed description of the model can be found in Ref. [15]. The currents are measured in $\mu\mathrm{A/cm}^2$ units and $C_m = 1\ \mu\mathrm{F/cm}^2$ is the membrane capacitance. The resulting equations are integrated using an adapted second-order Runge-Kutta method designed for stochastic differential equations [16], with a step size $dt = 0.01$ ms. The accuracy of the zero noise results was checked against results obtained with a smaller step size and using a fourth-order Runge-Kutta algorithm [17].

*Author to whom correspondence should be addressed. FAX: 858 455 7933. Email address: tiesinga@salk.edu

There were two types of noise models. The first was a white-noise current, i.e., $\langle \xi(t)\xi(t')\rangle = 2D\delta(t-t')$ (D is expressed in mV^2/ms) as in [18], and the synaptic current I_{syn} in Eq. (1) was set to zero. The second was a sum of inhibitory and excitatory conductances,

$$I_{syn} = g_e s_e(t)(V-E_e) + g_i s_i(t)(V-E_i), \tag{2}$$

where the maximum conductance is $g_e = g_i = 2.0$ mS/cm^2, and the reversal potentials are $E_e = 0$ mV and $E_i = -75$ mV, for the excitatory and inhibitory synapses, respectively. Unitary EPSPs (IPSPs) are modeled as quantal conductance increases, $\Delta s_e = 0.001$ ($\Delta s_i = 0.005$), in the synaptic kinetic variable $s_e(t)$ [$s_i(t)$]. The conductance pulses in $s_e(t)$ and $s_i(t)$ decay exponentially in time with a time constant $\tau_e = 2$ ms ($\tau_i = 10$ ms). The postsynaptic potentials are independent and Poisson-distributed with average firing rates f_e and f_i, respectively. For the simulations of the conductance-driven neuron, $I = 0.10$ μA/cm^2, yielding a resting membrane potential $V_{rest} = -62.305$ mV.

B. Mean and variance of the current for a conductance drive

The goal is to characterize the effects of the average synaptic drive and its variance. This is not as straightforward as in the white-noise case. The EPSPs and IPSPs open synaptic channels, and thus result in an increased conductance, a changed average driving current, and a new resting membrane potential. The statistical properties of the driving force I_{syn} are the mean,

$$\eta \equiv \langle I_{syn}\rangle = \beta_e\langle s_e\rangle + \beta_i\langle s_i\rangle, \tag{3}$$

with $\beta_e = g_e(E_e - V_{rest})$ and $\langle s_e\rangle = \tau_e f_e \Delta s_e$ (with similar expressions for the inhibitory part in this formula, and the ones that follow); and the variance,

$$\eta_2 \equiv \langle I_{syn}^2\rangle - \eta^2 = \Delta_e + \Delta_i, \tag{4}$$

with $\Delta_e = \frac{1}{2}\beta_e^2\langle s_e\rangle \Delta s_e$ and $\Delta_i = \frac{1}{2}\beta_i^2\langle s_i\rangle \Delta s_i$.

To keep η constant, with the membrane potential clamped at V_{rest}, it is necessary to covary Δf_e and Δf_i according to

$$\Delta f_e = -\frac{\beta_i \Delta s_i \tau_i}{\beta_e \Delta s_e \tau_e}\Delta f_i, \tag{5}$$

whereas to keep η_2 constant,

$$\Delta f_e = -\frac{\beta_i^2 \Delta s_i^2 \tau_i}{\beta_e^2 \Delta s_e^2 \tau_e}\Delta f_i. \tag{6}$$

Here we use $f_e = f_e^0 + \Delta f_e$ and $f_i = f_i^0 + \Delta f_i$, with initial presynaptic firing rates f_e^0 and f_i^0. Because of the effects of the synaptic conductances on the resting potential, and the possible generation of action potentials, the mean of the actual synaptic currents is not constant for constant η. (This would only be the case when the synaptic conductances are small compared to the leak conductance.) The quantities η and η_2, however, do have a clear experimental correlate. They are the mean and variance of the current that needs to be injected into a neuron to keep its voltage constant (voltage clamp) while receiving a specific synaptic drive. Here we investigate how this synaptic drive affects the dynamics of a current-clamped neuron as a function of η and η_2.

C. Calculated quantities

The raw data obtained from the simulations are the voltage $V(t)$ traces at discrete times $t = n\,dt$. The ith spike time is defined as the time t_i (expressed in ms) when the voltage crosses 0 mV from below. The ith interspike interval (ISI) is given by $\tau_i = t_{i+1} - t_i$. We calculate its mean, τ_{ISI}, and standard deviation σ_{ISI}. The coefficient of variation (C_V) is defined as the ratio $C_V = \sigma_{ISI}/\tau_{ISI}$. The firing rate in Hz is given by $f = 1000/\tau_{ISI}$. We also determined the interspike interval histogram (ISIH) in 500 bins of width $\Delta\tau = (50 - 400)dt$. We calculated the entropy S of the ISIH [19] when at least 99% of the intervals generated in the simulations are accounted for in the ISIH:

$$S = -\sum_i p_i \log_2 p_i + \log_2 \Delta\tau. \tag{7}$$

Here p_i is the numerical estimate for the probability of an ISI falling in bin i. The information rate R is S/τ_{ISI}.

We performed least-squares fits of the ISIH to a gamma probability distribution function, $P(t)$, with fitting parameters μ, r, and τ_d:

$$P(t) = \frac{(\mu r)^r (t-\tau_d)^{r-1} e^{-\mu r(t-\tau_d)}}{\Gamma(r)} \quad (t > \tau_d), \tag{8}$$

and P is equal to zero for $t \leq \tau_d$. The fitting parameters can be related to the moments of the distribution: $\tau_{ISI} = (1/\mu) + \tau_d$, $\sigma_{ISI} = 1/\mu\sqrt{r}$, and $C_V = 1/[\sqrt{r}(1+\mu\tau_d)]$.

We used both the Powell and Marquardt-Levenberg routines from Ref. [17] to minimize the square of the deviation between the fitting function and the data. A fit was acceptable when the average and variance of the ISIH and the fitting function differed less than 2%, the value of χ^2 (for optimal bin width, see [17]) was less than 2 and the parameters obtained by the different optimization routines differed by less than 10%.

III. RESULTS

A. White-noise-driven neuron

First consider the behavior of a white-noise-driven neuron as a function of the driving current I (Fig. 1). The rheobase is defined as the current I_{rheo} at which the neuron starts firing repetitively, here $I_{rheo} \approx 0.16$. For $D = 0$, the firing rate versus current (f-I) characteristic resembles a square-root function above the rheobase [20], and below the rheobase the firing rate is zero. There is low-frequency noise-induced spiking below the rheobase for $D = 0.004$. In that case, the C_V starts out at values close to 1 for currents near the rheobase, but quickly decreases with increasing current. For stronger noise, $D \geq 2$, the f-I is approximately linear over its entire range [21], and the C_V does not vary strongly with current.

We studied the output statistics as a function of D for two current values, $I = 0.16$, close to, but still below, the rheobase, and $I = 0.6$, above the rheobase (Fig. 2). The variance σ_{ISI} increases with increasing D for $I = 0.6$, but *decreases* for

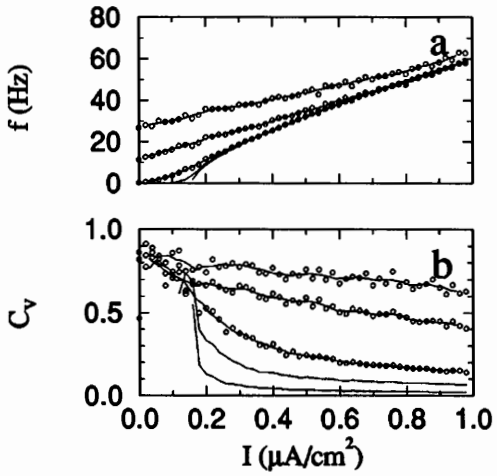

FIG. 1. White-noise-driven neuron. (a) The firing rate f, and (b) the coefficient of variation C_V as a function of injected current I. From top to bottom, the noise strength is $D=8$, 2, 0.2, 0.04, and 0.004. Averages are calculated over 20×10^3 ms after discarding a transient of 500 ms. The solid lines for $D=8$, 2, and 0.2 are running averages over four points. The original data points are plotted as small circles.

$I=0.16$. At the same time, the firing rate increases approximately as $\sqrt{D}$ for $I=0.16$, whereas it spikes repetitively at an approximately constant firing rate from $D=0$ to $D\approx1$ for $I=0.6$. The model neuron can thus be in two dynamical states depending on its input: For $I=0.16$, it is in the fluctuation-dominated state, and for $I=0.60$ ($D\ll1$), in the current-dominated state. These results are consistent with the theory presented in Ref. [20] for the excitable (fluctuation-dominated) and oscillatory (current-dominated) regime of their type-I neuron. We also determine the Shannon entropy [Eq. (7)] of the distribution of ISIs [Fig. 2(c)]. It represents the maximum amount of information that *in principle* can be coded in one interval [22,19]. For $I=0.16$ it decreases with D, whereas for $I=0.6$, it initially increases, and then converges to the $I=0.16$ result. The information capacity per interval for $I=0.16$ is higher compared to the capacity for $I=0.6$. However, the converse holds for the information rate R, since the firing rate for $I=0.6$ is higher.

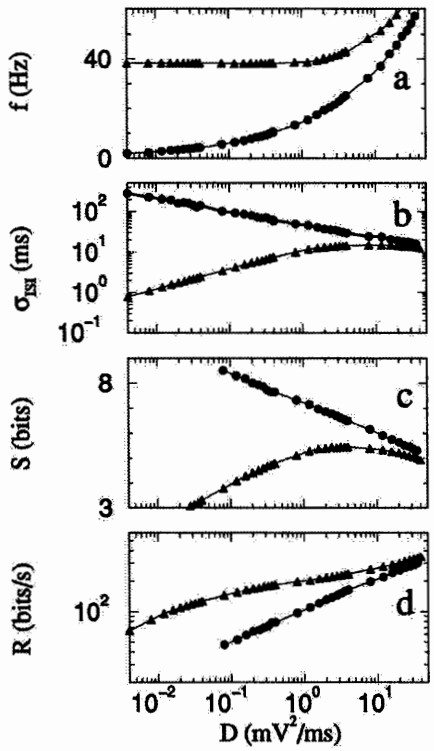

FIG. 2. White-noise-driven neuron. (a) The firing rate f, (b) the standard deviation σ_{ISI}, (c) the entropy S per interval, and (d) the entropy rate R versus noise variance D. We used $I=0.16$ (filled circles) and $I=0.60$ (filled triangles). Averages are calculated over 200×10^3 ms after discarding a transient of 5×10^3 ms.

In Fig. 3, five ISIHs with the corresponding voltage time traces are shown with D increasing from top to bottom. We fitted the ISIH to a gamma probability density function (pdf), given in Eq. (8). For $D=0.024$, the spike train is regular, the ISIH is sharp, and it is fitted by a gamma pdf of order $r>30$. In fact, a Gaussian distribution is also a good fit (not shown). For higher D values, the spike train is more variable and the ISIH is broader. The ISIH is also more asymmetric: the left-hand side of the ISIH is less stretched compared to its tail on the right-hand side. The r value of the fitting function decreases to approximately 3. For $D=36$, the neuron is in the fluctuation-dominated regime. The r value is close to 1, corresponding to a Poisson spike train, and the ISIH resembles an exponential distribution. However, the fit shown in Fig. 3(i) did not satisfy the criteria for a good fit (see Sec. II). The voltage trace for $D=36$ resembles those measured in *in vivo* experiments [23,24].

The entropy of the Gaussian, gamma, and exponential distributions are, respectively [19],

$$S_{\text{Gauss}}=\log_2\sigma_{\text{ISI}}+\tfrac{1}{2}\log_2 2\pi e, \tag{9}$$

$$S_{\text{gamma}}=\log_2\sigma_{\text{ISI}}+\log_2\Gamma(r)+[(1-r)\psi(r)+r]/\ln 2, \tag{10}$$

$$S_{\text{exp}}=\log_2\sigma_{\text{ISI}}+1/\ln 2. \tag{11}$$

Here Γ is the gamma function and ψ is its logarithmic derivative [25]. The entropy depends on σ_{ISI} as $\log_2\sigma_{\text{ISI}}$ with an additive constant that depends on the shape of the distribution. The Gaussian distribution has the highest entropy for a given variance: the additive constant is $\log_2 2\pi e\approx2.05$, compared to $1/\ln 2\approx1.44$ for the exponential distribution. The additive constant for the gamma pdf takes a value between the Gaussian and exponential result: for $r=1$, $S_{\text{gamma}}=S_{\text{exp}}$, and for large r, $S_{\text{gamma}}\to S_{\text{Gauss}}$. Therefore, there is an optimum in the entropy per interval in Fig. 2(c), since there is a maximum in σ_{ISI} itself [Fig. 2(b)] and the r value of the distribution decreases from $r>30$ to $r=1$.

B. Conductance-driven neuron

For the conductance-driven neuron, we use η and η_2 as parameters, but in the simulations we actually vary the presynaptic firing rates f_i and f_e. Since the firing rates are always positive, it is not possible to have a finite η while at the same time $\eta_2=0$. The current-dominated regime found in the white-noise-driven neuron for low variance and moderate mean is small in the conductance-driven neuron for the parameter values used here.

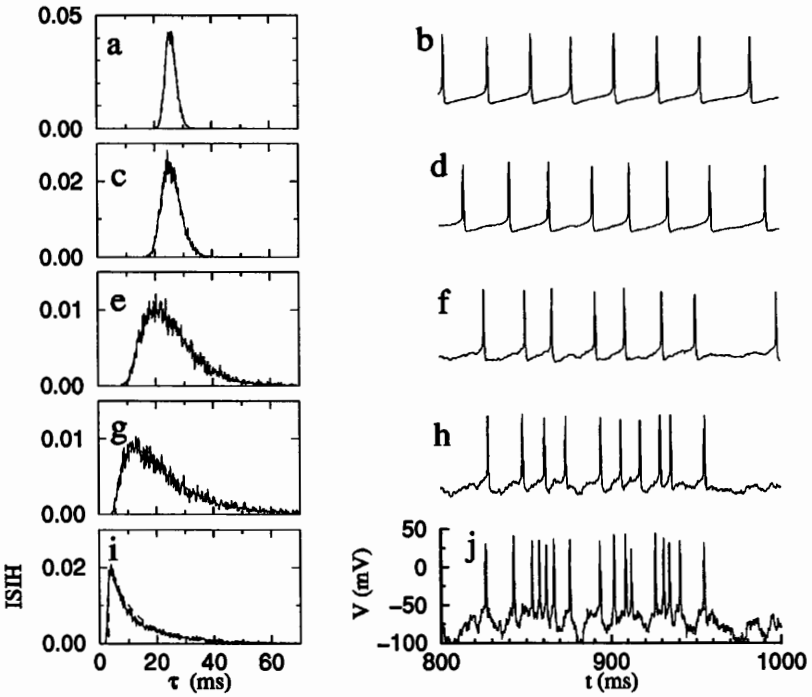

FIG. 3. White-noise-driven neuron. Left-hand side: ISIH (solid line), and the gamma probability density function fitted to it (dashed line) as a function of the interspike interval τ; right-hand side: corresponding voltage time traces. From top to bottom, $D=0.024$ (a,b), 0.08 (c,d), 0.8 (e,f), 4 (g,h), and 36 (i,j) with $I=0.6$. The fitting parameters are $(\mu,r,\tau_d,\chi^2)=(0.096,30.0,15.6,1.3)$, $(0.071,17.1,11.9,1.2)$, $(0.061,3.2,9.0,1.2)$, $(0.059,1.6,5.9,3.0)$, and $(0.10,1.0,3.2,4.2)$, respectively. See text for details. Averages are calculated over 200×10^3 ms after discarding a transient of 500 ms.

We first keep η_2 constant, and vary η. The results are similar to those in Fig. 1. The firing rate increases when increasing η, but the C_V and the entropy per interval decrease [Fig. 4(I)]. Note that the f-η characteristic is sublinear for small η [Fig. 4(Ia)].

The behavior for constant η and varying η_2 is shown in Fig. 4(II). The firing rate now *decreases* with increasing variance. This counterintuitive effect occurs because in order to increase the variance, more synaptic channels need to be opened. As a result, the total conductance increases (i.e., the input resistance is reduced), making it harder for the current to drive the neuron to a spiking threshold. Hence the firing rate decreases. The C_V increases with the variance η_2, as for the white-noise-driven neuron.

In Fig. 5 we show the ISIHs and the gamma-pdf least-squares fit. The r value of the fitting function decreases from approximately 3 to 1 with decreasing η. The first three fits have relatively high χ^2 values, due to significant deviations of the ISIH from a gamma pdf for large ISI values. However, the deviations for ISI values near the mode of the distribution are small and the fit appears reasonable.

C. Comparison of C_V-τ_{ISI} curves

In Fig. 6, we compare (a) the RW and IAF models, (b) the white-noise-driven, and (c) the conductance-driven neuron. We plot the C_V versus τ_{ISI} curves for constant mean of the

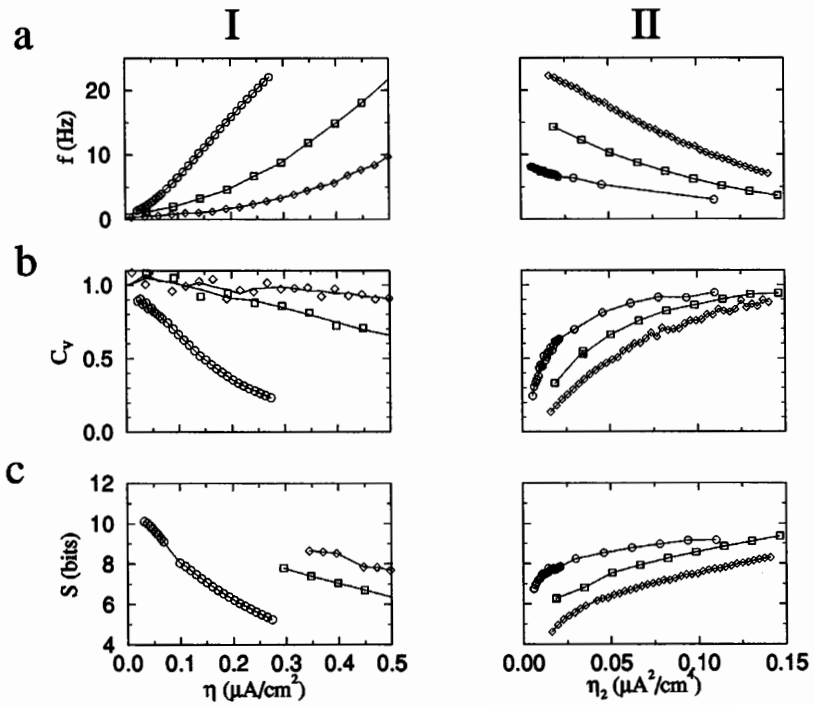

FIG. 4. Conductance-driven neuron. (a) The firing rate f, (b) the coefficient of variation C_V, (c) the entropy S per interval, versus (I) the mean drive η and (II) the variance of the drive η_2. Here (I) $\eta_2=0.0251$ (circles), 0.137 (squares), and 0.216 (diamonds); and (II) $\eta=0.0997$ (circles), 0.174 (squares), and 0.263 (diamonds). Averages are calculated over at least 200×10^3 ms after discarding a transient of at least 5×10^3 ms.

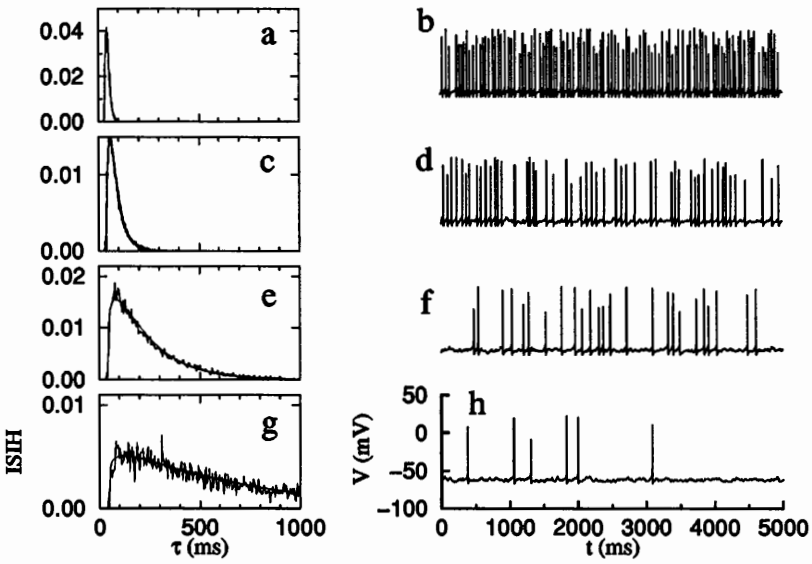

FIG. 5. Conductance-driven neuron. Left-hand side: ISIH (solid line), and the gamma probability density function fitted to it (dashed line) as a function of the interspike interval τ; right-hand side: corresponding voltage time traces. From top to bottom: $\eta=0.254$ (a,b), 0.151 (c,d), 0.069 (e,f), 0.023 (g,h) with $\eta_2=0.0251$. The fitting parameters are $(\mu,r,\tau_d,\chi^2)=(0.048,3.3,27.2,28)$, $(0.021,1.7,36.4,5.9)$, $(0.0051,1.3,43.9,2.44)$, and $(0.0015,1.1,52.0,1.1)$, respectively. See text for details. Averages are calculated over 5000×10^3 ms after discarding a transient of 5×10^3 ms. The action potentials appear to vary in amplitude. This is due to the undersampling of the voltage trace at 0.5 ms for display purposes.

current drive (solid lines), d, I, and η, respectively, and for constant variance (dashed lines), D, D, and η_2, respectively.

The mean and variance of the interspike intervals can be calculated analytically for the RW and perfect IAF model. For the RW model, we have [26].

$$\tau_{\mathrm{ISI}}=\frac{\theta}{d},$$

$$\sigma_{\mathrm{ISI}}=\frac{\theta D}{d^3}, \tag{12}$$

$$C_V=\sqrt{\frac{D}{\theta d}}=\sqrt{\frac{D\tau_{\mathrm{ISI}}}{\theta^2}}.$$

Here d is the mean and D the variance of the drive, and θ is the spiking threshold. In the perfect IAF model, the membrane potential does not decay in time, and the postsynaptic potentials are modeled as δ pulses with strength a_i and a_e, for inhibitory and excitatory pulses, respectively. In that case, Eqs. (12) also hold [26], with $d=a_e f_e-a_i f_i$ and $D=a_e^2 f_e+a_i^2 f_i$ and presynaptic firing rates f_i and f_e. In Fig. 6(a), we plot the constant D and d lines according to Eqs. (12). The solid curves in Fig. 6(a) are parallel to the C_V axis. The firing rate is constant; only the C_V increases with D. The dashed curves are convex, $C_V\sim\tau_{\mathrm{ISI}}^{1/2}$.

In Fig. 6(b) there are two types of solid lines. Solid lines that start at $C_V=0$ with a finite value of τ_{ISI} (current-dominated regime). On these lines the firing rate is constant while the C_V increases. However, for higher C_V values these lines curve towards the left of the graph: the C_V and the firing rate increase at the same time. The other solid line (we show only one example, denoted by an asterisk *) starts out at large τ_{ISI} values with a finite C_V value (fluctuation-dominated regime). The dashed lines all curve upwards; the C_V increases with increasing τ_{ISI}. Thus the same noise variance D leads to comparatively more jitter for lower firing rates.

For the conductance-driven neuron [Fig. 6(c)], the solid lines curve toward the right: the C_V and τ_{ISI} increase at the same time, because the firing rate decreases with variance [see also Fig. 4(a)]. The dashed curves are concave compared to convex in Figs. 6(a) and 6(b).

In summary, the most important difference between the four different neuron/driving force models is their behavior

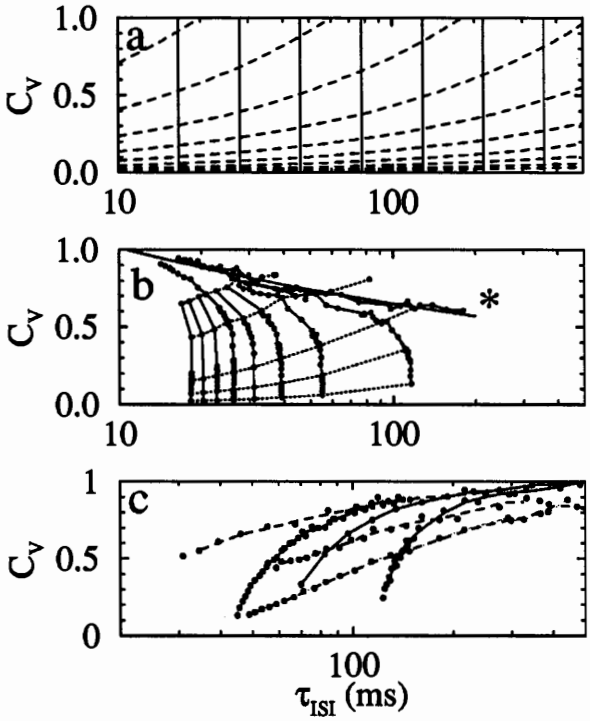

FIG. 6. The C_V versus τ_{ISI} curves for (a) RW and perfect IAF model, (b) white-noise-driven neuron, and (c) conductance-driven neuron. On the solid lines the mean current is kept constant, whereas on the dashed lines the variance is kept constant. The curves in (b) and (c) are obtained from numerical simulations, whereas those in (a) are the analytical results from Eq. (12). The parameter values in (b) are, for solid lines from right to left, $I=0.16$, 0.2, 0.3, 0.4, 0.5, 0.6, 0.7, 0.8, and 0.9; and for the dashed lines from bottom to top, $D=0.004$, 0.04, 0.20, 2.0, and 8.0. In (c) we have from right to left (solid lines), $\eta=0.10$, 0.17, and 0.2629; and from bottom to top (dashed lines), $\eta_2=0.015$, 0.025, and 0.041. Averages are calculated over at least 200×10^3 ms after discarding a transient of at least 500 ms.

as a function of the variance of the fluctuating current. For the white-noise-driven neuron, the firing rate increases with the variance, whereas in the conductance-driven neuron it decreases, and for the RW and perfect IAF models it remains the same.

IV. DISCUSSION

The model neuron can be in two different dynamical states that have clear physiological correlates. Neurons in the *in vitro* slice preparation are characterized by a low intrinsic noise level [27], and they receive little synaptic drive. This suggests that their dynamics is current-dominated. In contrast, *in vivo* neurons are constantly being bombarded by EPSPs and IPSPs, and fire at high C_V values [8]. Indeed, recent experiments show that the input resistance of cortical neurons *in vivo* can be up to five times lower than their input resistance in the absence of synaptic inputs [23,24]. The variance of the voltage fluctuations is also higher with synaptic inputs present [23,24]. This resembles the fluctuation-dominated conductance-driven state reported in this paper. In what follows, we discuss the functionally relevant differences between these two states and suggest future experiments.

The f-I in the current-dominated state is highly nonlinear. Close to the rheobase, a small increase in input current can lead to a large increase in firing rate. The f-I in the fluctuation-dominated state is linear for white-noise-driven neurons, and it can be sublinear for conductance-driven neurons. The dynamical range is much larger in fluctuation-dominated, conductance-driven neurons. As a result, cortical neurons are able to maintain their firing rate within a fixed range despite their constant synaptic bombardment and a wide range of input frequencies [8].

In the current-dominated state, the ISI are distributed according to a Gaussian, or gamma (with $r \gg 1$) [Eq. (8)], probability distribution. The information capacity of a Gaussian distribution is maximal at a given value for the variance σ_{ISI}. Therefore, the potential information content is maximal in the interspike intervals or, equivalently, in the instantaneous firing rate, $1/\tau_i$ (see Sec. II). In the fluctuation-dominated state, the ISI are distributed according to a gamma distribution with r values close to 1. A Poisson spike train ($r=1$) has the highest information rate per spike time at a given firing rate [28,19]. In the fluctuation-dominated state, therefore, the potential information content of the spike times is maximal. This suggests that the nature of information processing might be different in the fluctuation versus current-dominated states. It also lends support to the idea that the neuron can act as a rate coder or a spike-time coder depending on the input types.

Simple models, such as the perfect IAF and RW, were used in previous studies of neuronal variability [1,3,8]. These models can produce spike trains with almost any value for the firing rate and C_V for more or less realistic parameter values [9,10]. This approach is useful when considering a neuron in isolation. However, in a network of neurons it is also important to correctly model how a neuron responds to dynamical changes in the mean and variance of the fluctuating drive. Here we have shown that these models do not account for the variance effects of fluctuating currents that were observed in more realistic biophysical models. It is important to include the contributions of synaptic noise explicitly as synaptic conductances. Salinas and Sejnowski [29] have shown that the leaky IAF model can account for the variability observed in experiment [8] if synaptic conductances are included. An important issue is whether and to what extent that would change results obtained previously in networks of integrate-and-fire neurons without synaptic conductances, such as, for example, Refs. [8,30,31]. This remains for future study.

We have also studied the statistics of the output spike train of a biophysical model neuron as a function of the mean and variance of the stochastic driving current. As mentioned before, the input parameters have a clear experimental analog: they are the mean and variance of the injected currents in voltage-clamp mode that are necessary to keep the neuron at a constant membrane potential. However, during current-clamp mode the voltage is able to change according the neuronal dynamics, allowing the statistics of the output spike train to be determined. Using *in vivo* measurements of the mean and variance of the fluctuating current, and the distribution of EPSP and IPSP characteristics, one can estimate the presynaptic spiking rates f_i and f_e using Eqs. (3) and (4). The output statistics can subsequently be measured in the current-clamp mode. During *in vivo* experiments, however, one has relatively little control over the statistics of the synaptic inputs, but during *in vitro* experiments one can inject a current with arbitrary statistical properties. One of the key results in this paper is that the source of the variance matters: a current drive is different from a conductance drive. One therefore has to inject conductances into the neuron using the recently developed dynamic-clamp technique [32]. The C_V versus τ_{ISI} diagrams can then be reconstructed by systematically varying f_i and f_e. Can the *in vivo* dynamics of neurons be reproduced in the *in vitro* preparation by injecting synaptic conductances? Does the firing rate of neurons decrease when the variance of the fluctuating current is increased? Experiments are presently in progress to address these questions [33].

ACKNOWLEDGMENTS

We thank Jean-Marc Fellous and Emilio Salinas for helpful comments. Part of the numerical calculations has been performed at the High Performance Computer Center at Northeastern University. This work was supported by the Sloan Center for Theoretical Neurobiology at the Salk Institute, and the Center for Interdisciplinary Research on Complex Systems at Northeastern University.

[1] G.L. Gerstein and B. Mandelbrot, Biophys. J. **4**, 41 (1964).
[2] B.J. West and W. Deering, Phys. Rep. **246**, 1 (1994).
[3] R.B. Stein, Biophys. J. **5**, 173 (1965).
[4] W.R. Softky and C. Koch, J. Neurosci. **13**, 334 (1993).
[5] M.N. Shadlen and W.T. Newsome, Curr. Opin. Neurobiol. **4**, 569 (1994).
[6] W.R. Softky, Curr. Opin. Neurobiol. **5**, 239 (1995).
[7] M.N. Shadlen and W.T. Newsome, Curr. Opin. Neurobiol. **5**,

248 (1995).
[8] M.N. Shadlen and W.T. Newsome, J. Neurosci. **18**, 3870 (1998).
[9] T.W. Troyer and K.D. Miller, Neural Comput. **9**, 971 (1997).
[10] G. Bugmann, C. Christodoulou, and J.G. Taylor, Neural Comput. **9**, 985 (1997).
[11] D. Brown, J. Feng, and S. Feerick. Phys. Rev. Lett. **82**, 4731 (1999).
[12] P.H.E. Tiesinga and J.V. José, Neurocomputing **26-27**, 299 (1999).
[13] G.M. Shepherd, *Synaptic Organization of the Brain*, 4th ed. (Oxford University Press, Oxford, 1998).
[14] X.J. Wang and G. Buzsáki, J. Neurosci. **16**, 6402 (1996).
[15] P.H.E. Tiesinga and J.V. José, Network **11**, 1 (2000).
[16] H.S. Greenside and E. Helfand, Bell Syst. Tech. J. **60**, 1927 (1981).
[17] W.H. Press, S.A. Teukolsky, W.T. Vetterling, and B.P. Flannery, *Numerical Recipes* (Cambridge University Press, Cambridge, England, 1992).
[18] D. Golomb and J. Rinzel, J. Neurophysiol. **72**, 1109 (1994).
[19] T.M. Cover and J.A. Thomas, *Elements of Information Theory* (Wiley, New York, 1991).
[20] B.S. Gutkin and G.B. Ermentrout, Neural Comput. **10**, 1047 (1998).
[21] F.E. Theunissen, F.H. Eeckman, and J.P. Miller, in *Neural Systems: Analysis and Modeling*, edited by F. Eeckman (Kluwer Academic, Dordrecht, 1993), pp. 127–136.
[22] C.E. Shannon and W. Weaver, *The Mathematical Theory of Communication* (University of Illinois Press, Urbana, 1949).
[23] D. Pare, E. Shink, H. Gaudreau, A. Destexhe, and E.J. Lang, J. Neurophysiol. **79**, 1450 (1998).
[24] D. Pare and A. Destexhe, J. Neurophysiol. **81**, 1531 (1999).
[25] M. Abramowitz and I. Stegun, *Handbook of Mathematical Functions* (Dover, New York, 1974).
[26] H.C. Tuckwell, *Introduction to Theoretical Neurobiology I & II* (Cambridge University Press, Cambridge, England, 1988).
[27] Z.F. Mainen and T.J. Sejnowski, Science **268**, 1503 (1995).
[28] F. Rieke, D. Warland, R.R. de Ruyter van Steveninck, and W. Bialek, *Spikes: Exploring the Neural Code* (MIT Press, Cambridge, 1997).
[29] E. Salinas and T.J. Sejnowski, J. Neurosci. **20**, 6193 (2000).
[30] M.V. Tsodyks and T.J. Sejnowski, Network **6**, 111 (1995).
[31] C. van Vreeswijk and H. Sompolinsky, Science **274**, 1274 (1996).
[32] A.A. Sharp, M.B. O'Neil, L.F. Abbott, and E. Marder, J. Neurophysiol. **69**, 992 (1993).
[33] J.-M. Fellous, A. Destexhe, and T.J. Sejnowski, Abstr. Soc. Neurosci. **26**, 1623 (2000).